

Final Report: Part III

on

Contract DA-44-009-eng-405
Project 8-23-02-003

Khi-Ruey Tsai

September 15, 1953

Report No. 9

Final Report: Part III
RF Project 443

REPORT

By

THE OHIO STATE UNIVERSITY
RESEARCH FOUNDATION

COLUMBUS 10, OHIO

Cooperator ENGINEER RESEARCH AND
DEVELOPMENT LABORATORIES;
Fort Belvoir, Virginia
Contract DA-44-009eng 405
Project 8-23-02-003
Investigation of PHOTOEMISSIVE
SURFACES

Subject of Report Part III of Final Report.
The Crystal Structure
of Cesium Monoxide.

Submitted by Kh1-Ruey Tsai

Date Sept 15, 1953.

UNOFFICIAL COPY

FOR INFORMATION ONLY

CONTENTS

	<u>Page</u>
List of Figures	iii
List of Tables	iv
INTRODUCTION	1
EXPERIMENTAL	1
(A) Preparation and Analysis of Cesium Monoxide.	1
(B) Re-examination of the Powder Pattern.	2
(C) Single Crystal Work.	7
TREATMENT OF THE SINGLE CRYSTAL DATA	12
(A) The Absorption Factor.	12
(B) The Temperature Factor and the Scale Factor.	12
ELECTRON DENSITY LINE SECTIONS	14
DISCUSSION	21
(A) Temperature Factor and Lattice Disorder.	21
(B) Extinction Arising from Partial Perfection of the Layer Crystal Along the C-axis.	22
(C) Polarization of the Cesium Ions in the Layer Lattice.	22
(D) Extra Powder Lines of Impure Cesium Monoxide Sample.	24
SUMMARY	26
APPENDIX	27
References	32

FIGURES

<u>Fig. No.</u>	<u>Title</u>	<u>Page</u>
1	Powder Photographs.	4
2	Dimensions of the Single Crystal Used for the Rotation Photographs.	8
3	Rotation Photographs, (3a, 3b, 3c).	9, 10, 11
4	Absorption Factors Vs. ρ -Indices.	13
5	Electron-Density Line Sections.	19

TABLES

<u>Table No.</u>	<u>Title</u>	<u>Page</u>
I	X-ray Powder Data for Cesium Monoxide.	5, 6
II	Observed and Calculated Structure Factors.	15, 16, 17, 18
III	Interatomic Distances of Cs_2O and CdCl_2 -type Layer Crystals.	25

FINAL REPORT PART III

THE CRYSTAL STRUCTURE OF CESIUM MONOXIDE

by Khi-Ruey Tsai

INTRODUCTION

The monoxide of cesium, Cs_2O , is believed to have played an important role in the Cs-O-Ag photocathode, although no investigation of the photoelectric property of the pure oxide has been recorded in the literature. The oxide, orange yellow at room temperature, is known to exhibit pronounced color changes upon heating and cooling^{1,9}. A theoretical understanding of these unusual properties will rely, first of all, upon a complete knowledge of the crystal structure of this oxide. It is interesting to note that this oxide is the only compound which has been assigned an anti- CdCl_2 type layer structure⁵, just as silver subfluoride, Ag_2F , is the only compound known to have an anti- CdI_2 type layer structure¹¹. However, there has been some doubt about the assigned structure of Cs_2O in so far as it is based upon not too precise x-ray powder work¹². More recently, Brauer¹ has observed some weak powder lines of the monoxide which can not be indexed by Helms and Klemm's model⁵. A further study of the structure of this oxide by means of single crystal work thus appeared to be desirable.

EXPERIMENTAL

(A) Preparation and Analysis of Cesium Monoxide

The monoxide was prepared by distilling a suboxide of cesium, Cs_7O_2 , in a pyrex vessel at 180 - 190°C until no more cesium appeared to condense on the air-cooled trap. The suboxide, Cs_7O_2 , in turn, was prepared by direct combination of stoichiometric proportions of pure cesium and pure oxygen in the presence of a small amount of purified argon, the procedure being the same as described for the preparation of tricesium monoxide, Cs_3O (of Part IV of this final report series).

The monoxide thus obtained was in the form of polycrystalline, laminated plates, orange-yellow at room temperature, cherry-red above 180°C and lemon-yellow at dry-ice temperature. It was readily pulverized by shaking with glass beads in a thoroughly degassed pyrex tube.

Because of the small weight percentage of oxygen in cesium monoxide, the composition of the sample can not be accurately determined by alkalimetric determination of the cesium content alone; for a $\pm 0.1\%$ error in the alkalimetric determination would give rise to a $\pm 2\%$ error in the indirectly calculated oxygen content. Thus both Rengade⁹ and Brauer¹ reported a cesium content of 94.4% for their Cs₂O samples; compared with 94.3% Cs required by the formula the analysis indicates an error of 2% in the ratio of gram atoms Cs to gram atoms oxygen. The indication of a cesium excess is not reliable since the difference is within experimental error.

However, assuming the absence of foreign elements, the monoxide sample can be accurately analyzed by decomposition with water and measurement of any small amount of gas evolved. If the sample contains excess cesium, or excess oxygen, this will liberate an equivalent amount of hydrogen, or oxygen, respectively, upon decomposition with water; the gas sample can be readily identified by means of a mass spectrograph or by the known methods of gas analysis and identification.

A sample of cesium monoxide thus analyzed gave 0.001 mol of gas for each mol of the monoxide, showing an almost stoichiometric compound. A separate preparation yielded a monoxide sample containing 2.8% excess oxygen because of a small leakage of atmospheric oxygen into the sample tube. This latter sample showed some weak extra lines on the x-ray powder photograph. However, both samples were found to be diamagnetic with $\chi_g \approx -0.20 \times 10^{-6}$ c.g.s.u.

(B) Re-Examination of the Powder Pattern

The finely pulverized sample was preserved in a thin-wall pyrex capillary of about 0.2 mm diameter. The powder pattern was first re-examined, using CuK α radiation and an 11.4-cm camera. The higher resolution

of the camera made it possible to observe many more weak powder lines besides those observed by Brauer. However, a careful examination of the powder pattern showed that it still could be indexed by the rhombohedral system with a c/a ratio of 4.46, instead of 2.30 originally employed by Helms and Klemm. (The weak powder lines observed were those with odd hexagonal h -indices.) Note that Helms and Klemm's c/a ratio was based upon a rhombohedral pseudo-cell containing one Cs^+ ion. This requires that the parameter of the Cs^+ ions in the true rhombohedral cell containing one Cs_2O 'molecule' be exactly $1/4$; i.e. 2Cs^+ at $\pm (1/4, 1/4, 1/4)$, a body-centered rhombohedral setting. The presence of weak powder lines with odd hexagonal h -indices shows that $1/4$ can not be the correct parameter.

From the present powder data, the hexagonal unit-cell dimensions were found to be: $a = 4.256 \pm 0.004 \text{ \AA}$ and $c = 18.99 \pm 0.02 \text{ \AA}$. For one Cs_2O 'molecule' per unit-cell (rhombohedral), the calculated density is 4.71 g/cc as compared with 4.60 g/cc observed by Helms and Klemm².

When a freshly pulverized sample was used, the powder lines contributed from lattice planes parallel, or nearly parallel, to the c -axis (i.e. the $hk\cdot l$ -type powder lines with zero or small l -indices) became considerably weakened, indicating a shearing disorder in the directions parallel to the basal plane while the $00\cdot l$ reflection became stronger, probably due to further slight cleavage along the basal planes with the resulting decrease in primary extinction of the $00\cdot l$ reflections. These statements are well illustrated by Fig. 1. The relative intensities of the lines in photograph *c* are in several instances quite different from the relative intensities of the corresponding lines in *a* and *b*. Indices and relative intensities of the powder lines of Fig. 1*b* are given in Table I. By reference to Table I the indices of the Cs_2O powder lines of Fig. 1 can be readily recognized. The intensity distribution of the powder photograph became normal again if the sample was heated for about an hour at 1500°C , or simply allowed to stand at room temperature for a few days and then photographed. This, together with the fact that the monoxide tends to crystallize in laminated plates with more or less perfect basal cleavage, leaves little doubt that a layer structure is correct.

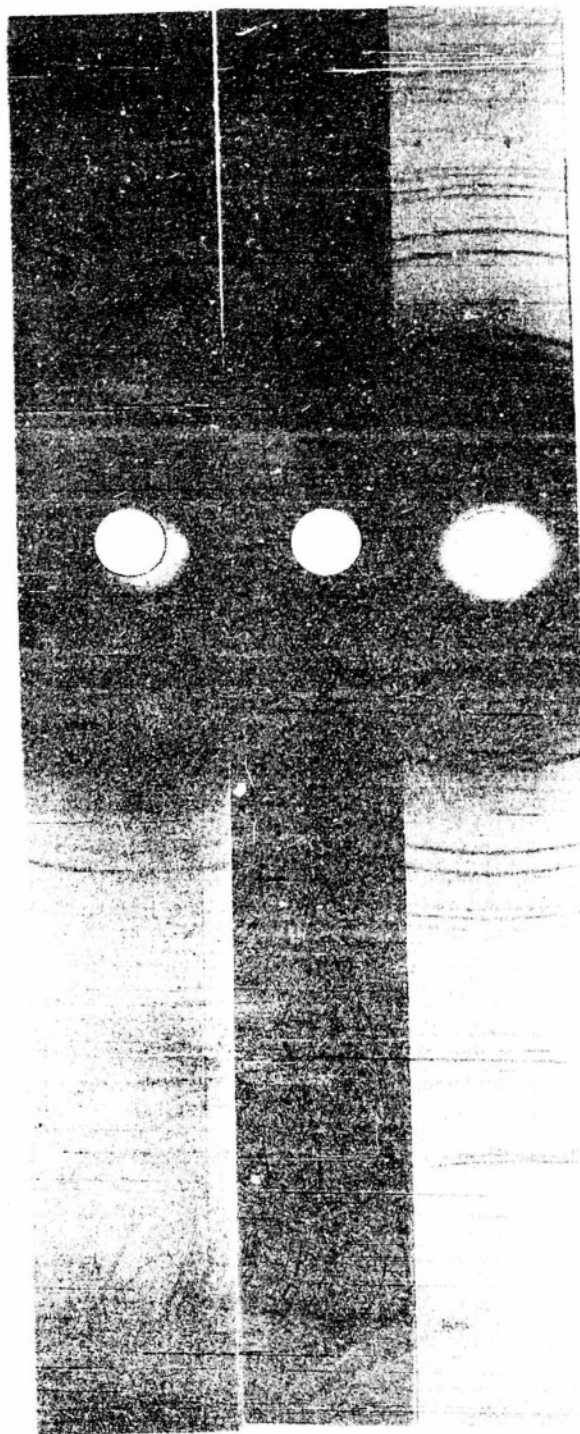


FIG. 1. X-ray ($\text{CuK}\alpha$) Powder Photographs of Cesium Monoxide. (a) Sample Containing 2.8% Excess Oxygen. (b) Pure Sample (99.8% Cs_2O). (c) Freshly Pulverized Sample.

TABLE I. X-RAY POWDER DATA
FOR CESIUM MONOXIDE

Hexagonal Indices hkl	Rhombohedral Indices HKL	d _{obs.}	d _{calc.}	I _{obs.}	I _{calc.} a=0.256 a=0.255	
0003	111	6.33	6.330	5	6.2	5.0
1011	100		3.620		0.2	0.3
1012	110	3.433	3.435	100	100	100
0006	222	3.159	3.165	25	26	27
1014	211	2.911	2.911	100	88	88
1015	221	2.638	2.643	1	0.9	0.5
1017	322	2.177	2.185	3	3.5	2.6
1120	101	2.124	2.128	25	35	35
0009	333		2.110		0.8	0.5
1123	210		2.017		1.4	1.1
1018	332	1.995	1.995	20	24	25
2021	111		1.835		0	0.1
2022	200	1.806	1.810	10	16	16
1126	321	1.766	1.766	20	29	29
2024	220	1.717	1.718	10	17	17
10110	433	1.688	1.688	10	11	11
2025	311		1.684		0.3	0.2
00012	444	1.580	1.583	5	3.5	3.7
10111	443	1.559	1.563	2	2.4	1.8
2027	331		1.525		1.0	0.7
1129	432	1.497	1.498	1	1.7	1.1
2028	422	1.457	1.456	5	8.8	9.2
2131	201		1.390		0	0
2132	211	1.378	1.379	10	14	14
10113	544	1.359	1.359	1	1.3	0.9
2134	310	1.336	1.337	10	14	14
20210	442	1.324	1.323	3	4.9	5.1
2135	320		1.308		0.3	0.2
10114	554	1.269	1.273	20	3.9	4.3
11212	543		1.270		10	11

TABLE I. (Continued)

Hexagonal Indices hkl	Rhombohedral Indices HKL	d _{obs.}	d _{calc.}	I _{obs.}	I _{calc.} u=0.256 w=0.255
00015	555		1.266		0.6
20211	533		1.260		1.1
2137	421		1.239		1.0
3030	211	1.229	1.229	3	5.6
3033	300		1.206		0.2
0333	221				0.1
2138	431	1.201	1.202	10	9.1
3036	411		1.146		7.0
0336	330	1.144		5	0.8
20213	553		1.145		0.6
10116	655	1.125	1.129	2	2.8
21310	532		1.123		6.1
20214	644	1.093	1.093	1	2.4
11215	654		1.088		2.5
21311	542		1.085		1.5
10117	665	1.069	1.069	1	1.2
2270	202		1.064		3.8
3039	522		1.062		0.6
0339	441				0.4
00018	666		1.055		0.6
2213	311		1.049		0.2
3141	212		1.021		0
3142	301	1.015	1.017	1	6.0
2216	420		1.009		5.6
21313	643		1.009		1.3
3144	321	0.998	0.999	2	6.9
20216	664		0.998		2.4

(C) Single-Crystal Work

Single crystals of Cs_2O were obtained by distilling a suboxide of cesium (Cs_7O_2) in pyrex capillaries at $170 - 180^\circ\text{C}$. The orange-yellow crystal used in the present investigation was a thin, almost rectangular plate, $0.14(2) \text{ mm} \times 0.20(4) \text{ mm} \times 0.03(4) \text{ mm}$, minus one small corner corresponding to about 3.5% of the total volume (Fig. 2). The two developed faces were identified as the 000ℓ basal planes; the remaining faces were formed by two $1\bar{1}20$ -planes, two 1104 -planes, and a $10\bar{1}0(?)$ plane which truncated a small corner of the plate. The following rotation photographs were taken: (1) CuK_α radiation with the hexagonal base diagonal, $(1\bar{1}20)$, $a' = \sqrt{3}a$, as the rotation axis; (2) CuK_α radiation with the hexagonal a -axis, $(10\bar{1}0)$, as the rotation axis; and (3) MoK_α radiation with the hexagonal a -axis, $(10\bar{1}0)$, as the rotation axis. The rotation spots were readily indexed; and the relative intensities were estimated visually by comparison with a blackening scale and measurement of the areas.

The rotation photographs (see Fig. 3) exhibit layer-shearing disorder similar to that of brucite, $\text{Mg}(\text{OH})_2$, a cadmium iodide type layer crystal, recently discussed by Brindley and Ogilvie². On both the a -axis rotation photograph, and the base-diagonal rotation photograph, the $hk\cdot 0$ -reflections appear as sharp spots, while the $00\cdot\ell$ -reflections appear as extended arcs. However, the degree of shearing disorder in the Cs_2O crystal employed appears to be small, the angular displacement of the c -axis being only about 2° as estimated from the vertical lengths of the $00\cdot\ell$ -spots.

Lane photographs taken along the c -axis, consisting essentially of streaks because of the slight shearing disorder, indicate a D_{3d} diffraction symmetry. This confirms the D_{3d} rhombohedral space group, there being only one Cs_2O 'molecule' per unit cell.

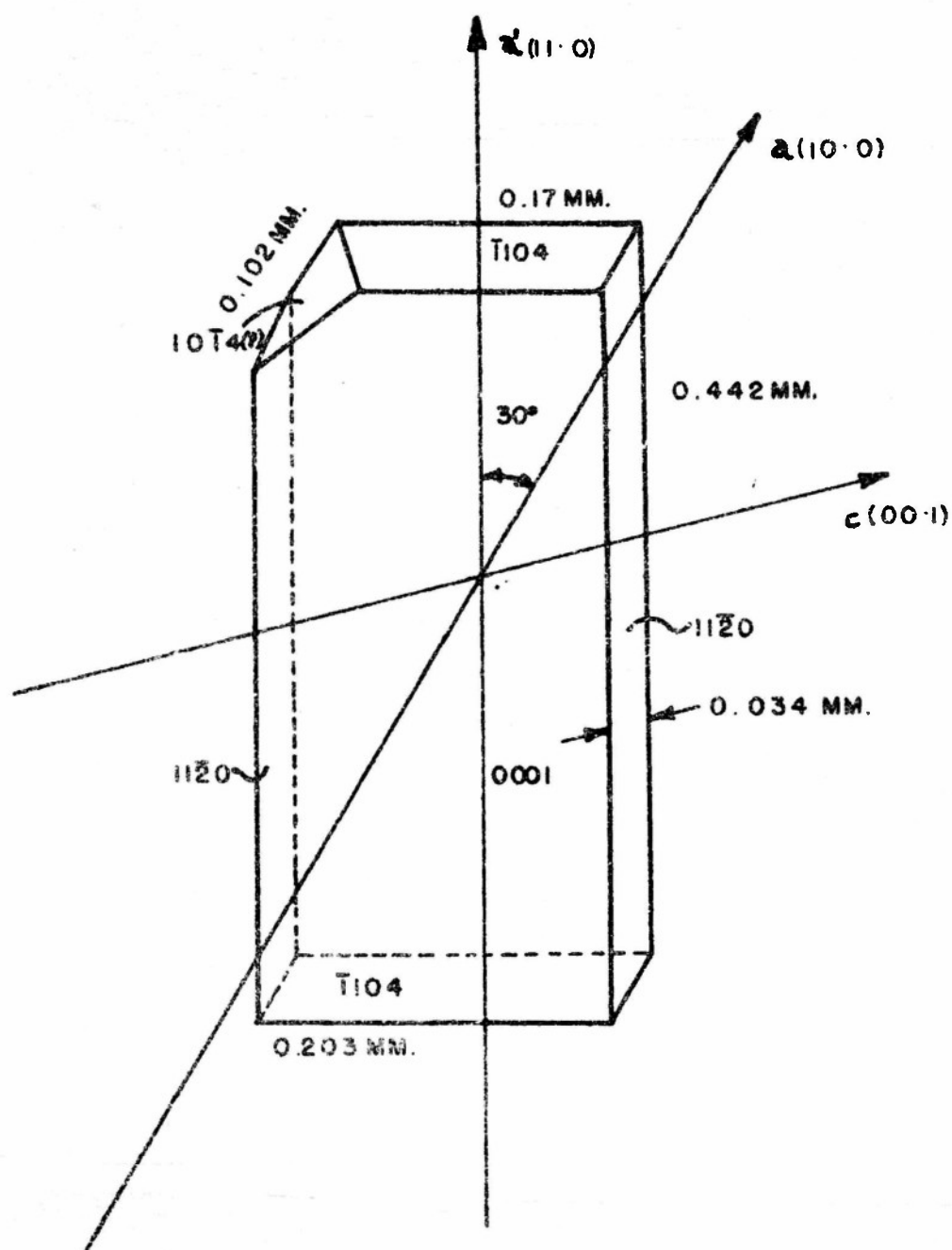


FIG. 2. Dimensions of the Single Crystal Used for the Rotation Photographs.



FIG. 3a. Single-Crystal Rotation Photograph.
CuK α -Radiations, Rotation About
(1120)-Axis.

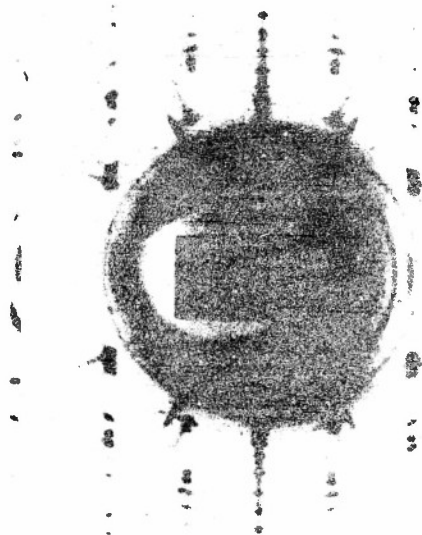


FIG. 3b. Single-Crystal Rotation Photograph.
MoK α -Radiations, Rotation about
(1010)-Axis.

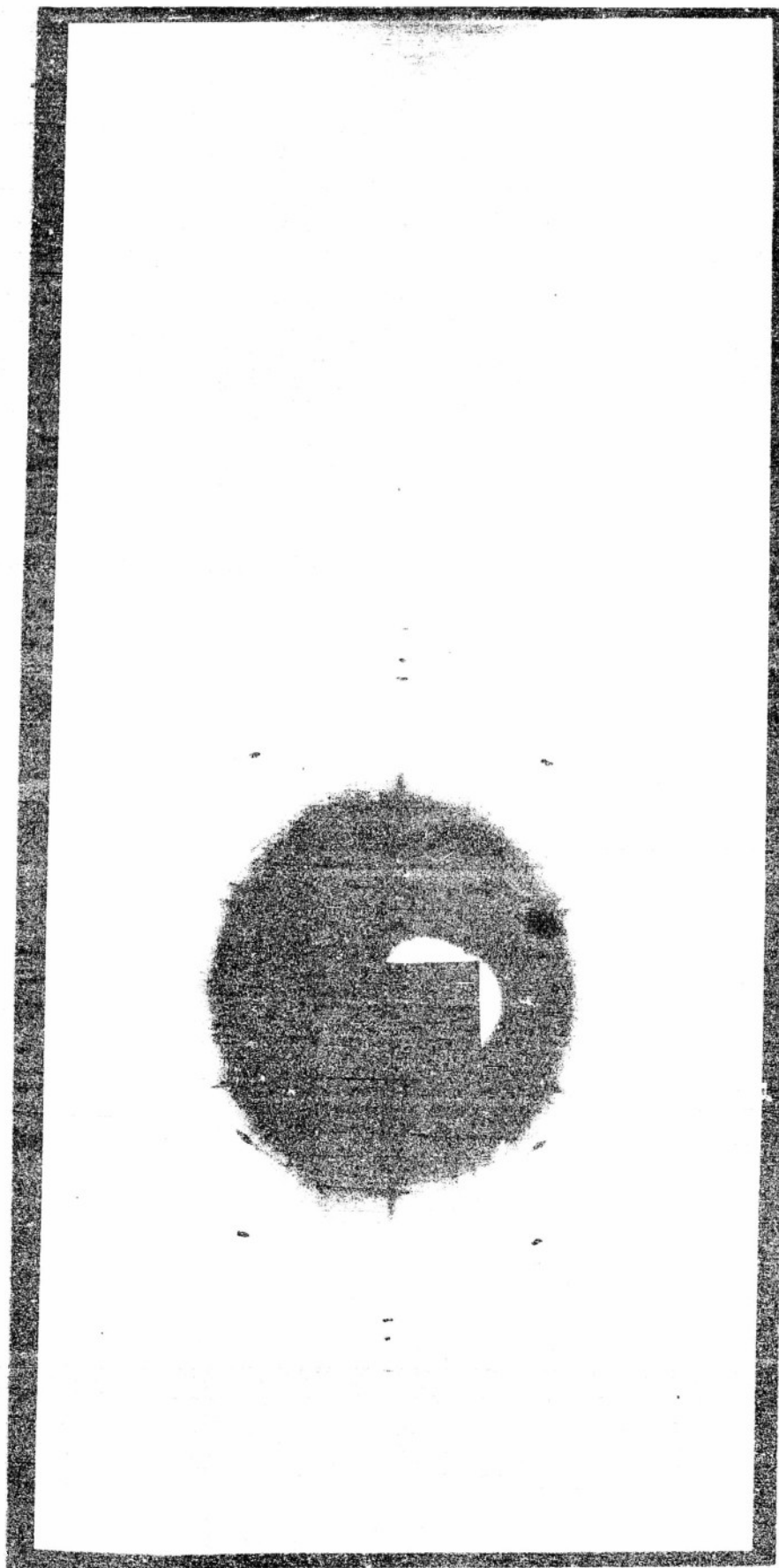


FIG. 3c. Single-Crystal Rotation Photograph.
CuK α -Radiation, Rotation about
(1010)-Axis.

TREATMENT OF THE SINGLE-CRYSTAL DATA

(A) The Absorption Factor

For a crystal containing a high percentage of heavy atoms, the absorption correction becomes very important. Hendershot⁷ has described an analytical method for computing the absorption factor for a rotating crystal bounded by polygonal faces. The equations apply to the zero-layer reflections only. Furthermore, in his treatment, internal reflections through nonadjacent faces are assumed to be negligible; obviously, this condition is not met with in the case of thin crystalline plates. The graphical method recently described by Howells⁸ requires considerable labor even for the case of constant cross section.

For a thin crystalline plate with rectangular cross section, a simple analytical treatment of the absorption factor can be obtained by dividing the cross section into appropriate regions for integration. For a detailed description of the method employed, see Appendix I. The absorption factors calculated as described in Appendix I are shown in Fig. 4.

(B) The Temperature Factor and the Scale Factor

The anti- CdCl_2 structure (D_{3d}^5) has only one variable parameter: 0^z at $0, 0, 0$; 2Cl^z at $\frac{1}{2}(u, u, u)$. The present powder data show that u is closer to 0.256 than to $1/4$ as reported by Helms and Klemm. From the single crystal intensity data, the observed structure amplitudes, Φ , (including the inherent temperature factor and the scale factor) were calculated, taking $\Phi_{110} = 85$ as an arbitrary basis in order to give a scale factor, K , close to unity. Based upon these values of Φ , an electron-density line-section through the c -axis was constructed and u was again found to be close to 0.256. The structure factors, F_c , for $u = 0.255$ and $u = 0.256$ were then calculated using Thomas-Fermi scattering factors for cesium and oxide ions. The latter value of u gave slightly better agreement with the observed F_{obs} . A least squares treatment of the values of (Φ/F_c) versus corresponding values of $\sin^2 \theta/\lambda^2$

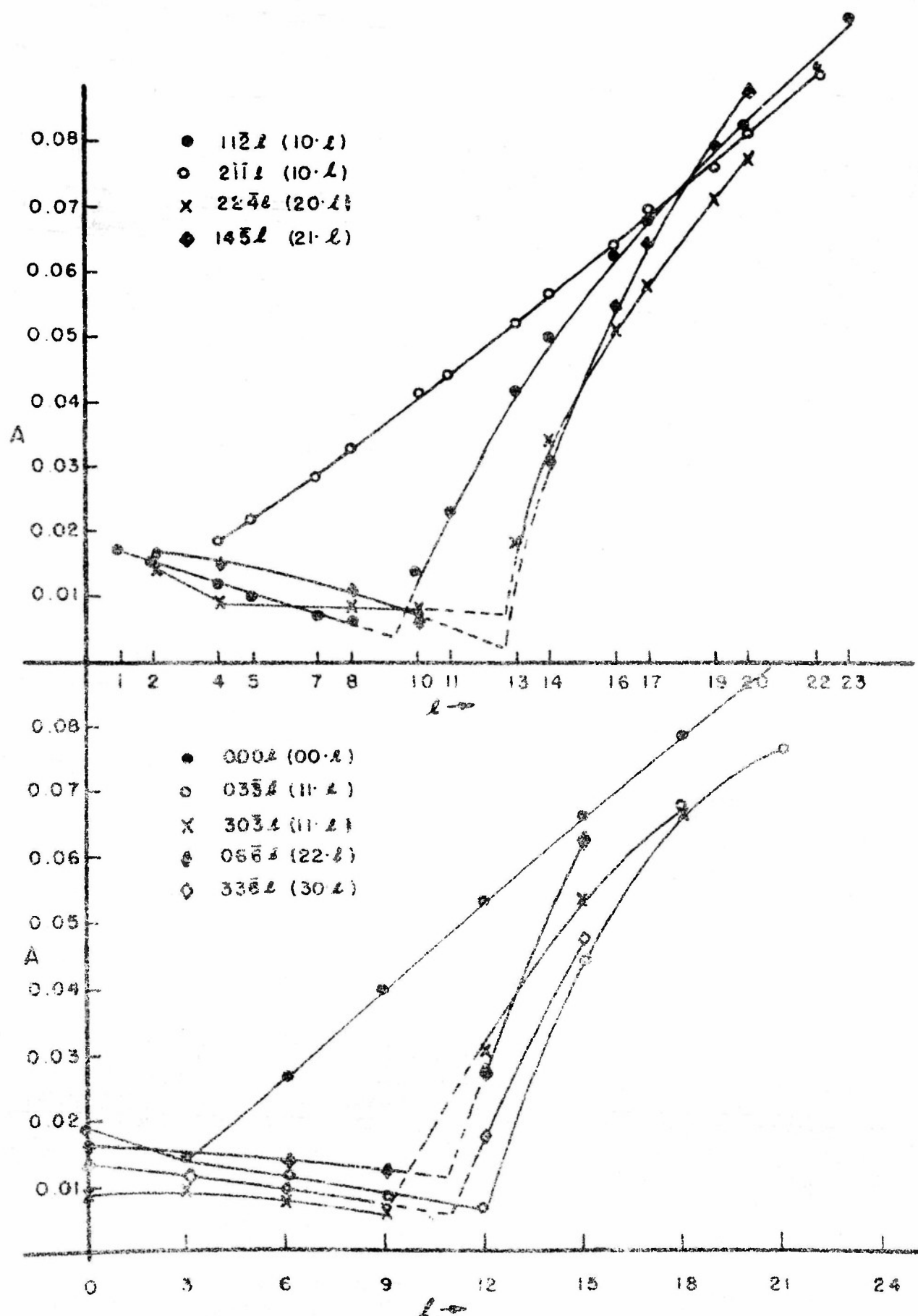


FIG. 4. Absorption Factors Versus l -Indices for Rotation Photograph (a).

gave $K = 0.829$ and $B_T = 3.24 \times 10^{-16} \text{ cm}^2$. Using these values of K and B_T , the observed structure factors, F_o , (temperature factor taken out) were calculated from ψ by means of the expression, $\psi = KF_o \exp(-B_T \sin^2 \theta / \lambda^2)$. The reliability factor, $\sum (F_o - F_c) / \sum F_c$, was found to be 12.4% (see Table II).

ELECTRON-DENSITY LINE SECTIONS

Four line sections, $\rho(00z)$, of electron density along the c -axis were constructed from the following sets of data: (1) observed structure amplitudes including the natural temperature factor,

$$F_o' = \psi / K = F_o \exp(-B_T \sin^2 \theta / \lambda^2);$$

(2) calculated structure amplitudes,

$$F_c' = F_c \exp(-B_T \sin^2 \theta / \lambda^2)$$

based upon $u = 0.256$ and Thomas-Fermi's scattering factors for O^2 and Cs ; (3) calculated structure amplitudes based upon $u = 0.256$ and Pauling-Sherman's scattering factors for O^2 and Cs ; (4) observed structure amplitudes, F_o' , plus calculated values, F_c' , for the weak, unobserved reflections. These four sets of data cover the same region from $(\sin \theta) / \lambda = 0$ to $(\sin \theta) / \lambda = 0.542$, so the series termination errors in $\rho(00z)$ may be assumed to be approximately the same.

The calculated electron density line section, $\rho(00z)$, based on (3) shows a slightly higher oxygen peak and a slightly lower cesium peak than does $\rho_c(00z)$ based on (2). Otherwise there is no essential difference between the two line sections. Hence it is sufficient to use only the $\rho_c(00z)$ based on Thomas-Fermi F_c' for comparison with the observed electron density line sections, $\rho_o(00z)$, based on (1) and (4).

The three line sections based on (1), (2), and (4) show practically the same oxygen peak and the same position for the maximum of the cesium peak (see Fig. 5). Hence $u = 0.256 = 15.36/60$ is the correct parameter. Up to a radius of about 0.7\AA from the center of the

TABLE II. OBSERVED AND CALCULATED
STRUCTURE FACTORS

The radiation is $K\alpha$ for both Cu and Mo.

hk \cdot l	$I_{\text{obs.}}$	Layer and Rotation Axis	Radi- ation	A	$\frac{1}{3}F_o$	$\frac{1}{3}F_K$	$\frac{1}{3}F_o$	$\frac{1}{3}F_c$
$\mu = 0.256$								
00 3	1.8	0, a'	Cu	0.0136	7.0	8.4	8.6	20
10 1								3.3
10 2	200	1, a'	Cu	0.0154	91	106	114	-87
	122	0, a	Mo	0.54	84			
00 6	100	0, a'	Cu	0.026	54	65	70	-84
	100	0, a	Cu					
10 4	92	1, a'	Cu	0.0114	79	99	109	96
	92	0, a	Mo	0.48	84			
10 5								-11
10 7	2.2	2, a'	Cu	0.028	13	21	24	27
	2.9	0, a	Mo	0.38	20			
11 0	141	0, a'	Cu	0.019	89	103	123	88
	134	3, a'	Cu	0.0086	80			
	93	1, a	Mo	0.57	85			
00 9	9.0	0, a'	Cu	0.040	15	18	22	-23
11 3	3.1	0, a'	Cu	0.0136	13	14	18	14
	3.4	3, a'	Cu	0.0086	11			
10 8	7.5	1, a'	Cu	0.0061	41	57	69	82
	32	2, a'	Cu	0.033	47			
	18	0, a	Mo	0.35	52			
20 1								1.1
20 2	45	2, a'	Cu	0.0146	64	75	96	-74
	34	0, a	Mo	0.56	60			
11 6	37	0, a'	Cu	0.0214	52	59	77	-71
	18	3, a'	Cu	0.0086	39			
	50	1, a	Mo	0.46	55			
20 4	22	2, a'	Cu	0.0089	59	70	92	79
	28	0, a	Mo	0.54	57			
10 10	11	1, a'	Cu	0.0143	35	41	55	-67
	15	2, a'	Cu	0.040	33			
	4.6	1, a	Mo	0.23	34			
20 5								-10
00 12	39	0, a'	Cu	0.053	38	45	62	70
	cat. 4	0, a	Mo	0.24	36			
10 11	3.9	1, a'	Cu	0.024	18	22	30	33
	4.1	2, a'	Cu	0.045	18			

TABLE II. (Continued)

hk.l	I _{obs.}	Layer and Rotation Axis	Radi- ation	A	$\frac{1}{3}\psi$	$\frac{1}{3}\bar{\psi}$ K	$\frac{1}{3}F_o$	$\frac{1}{3}F_c$ u:0.256
20 ca 7	1.0	0, a	Mo	0.27				
11 9	2	0, a	Cu		15	18	26	22
	0.6	0, a'	Cu	0.0089	8.4	13	19	-21
	3.4	3, a'	Cu	0.0058(?)	(21)			
	1.9	1, a	Mo	0.39	13			
20 8	5.0	2, a'	Cu	0.0089	33	45	65	70
	9.6	0, a	Mo	0.46	40			
21 1								0.4
21 2	17	1, a'	Cu	0.018	46	55	85	-65
	15	1, a	Mo	0.55	45			
10 13	4.9	1, a'	Cu	0.033	18	21	32	-29
	3.8	2, a'	Cu	0.053	17			
	0.6	0, a	Mo	0.25	15			
21 4	11.4	1, a'	Cu	0.015	42	49	78	70
	11	1, a	Mo	0.54	40			
20 10	ca 1.5	2, a'	Cu	0.0079		34	54	-60
	4.1	0, a	Mo	0.43	28			
21 5								-10
10 14	16	1, a'	Cu	0.050	28	35	58	-54
	10	2, a'	Cu	0.057	30			
11 12	ca 2.6	0, a'	Cu	0.0064	27	35	58	62
	27	3, a'	Cu	0.030	30			
00 15	ca 2.6	0, a'	Cu	0.066		18	30	38
	3.6	0, a	Cu		15			
	ca 0.4	0, a	Mo	0.29	(16)			
20 11	ca 0.5	0, a	Mo	0.41	11	13	22	29
21 7	0.3	1, a	Cu		13	13	22	19
	0.4	1, a	Mo	0.50	9			
30 0	7.7	3, a'	Cu	0.0136	33	43	74	67
	8.4	0, a	Mo	0.55	38			
30 3	0.7	0, a	Cu		5	6	11	10
21 8	3.5	1, a'	Cu	0.0107	29	36	63	63
	5.2	1, a	Mo	0.49	31			
30 6	6.1	3, a'	Cu	0.0093	27	31	58	-58
	6.2	0, a	Mo	0.51	25			
20 13	1.5	2, a'	Cu	0.019	14	17	31	-27
10 16	12	1, a'	Cu	0.063	23	29	55	53

TABLE II. (Continued)

hk.l	I _{obs.}	Layer and Rotation Axis	Radi- ation	λ	$\frac{1}{3}\psi$	$\frac{1}{3}\bar{\psi}$ K	$\frac{1}{3}\tau_0$	$\frac{1}{3}\tau_c$ u=0.256
21 10	7.2	2,a'	Cu	0.064	25			
20 14	1.3	1,a'	Cu	0.0064	24	29	55	-55
21 11	6.4	2,a'	Cu	0.035	22	27	52	-50
11 15	1.3	0,a	Mo	0.35	21			
21 11	ca. 0.4	1,a	Mo	0.44	10	12	24	27
11 15	ca. 0.6	1,a	Mo	0.25	18	18	36	35
	4.2	0,a'	Cu	0.044	12			
	16	3,a'	Cu	0.054	18			
10 17	6.3	1,a'	Cu	0.058	16	22	44	-34
	4.5	2,a'	Cu	0.070	19			
22 0	3.8	0,a'	Cu	0.017	26	31	64	62
20 9								-18
00 18	6.5	0,a'	Cu	0.079	16	19	40	-44
22 3								9
31 1								-0.2
31 2	3.4	2,a'	Cu	0.016	24	29	63	-56
	2.3	1,a	Mo	0.54	23			
22 6	3.5	0,a'	Cu	0.014	18	22	48	-54
21 13								-25
31 4	2.1	1,a	Mo	0.54	22	27	60	59
20 16	ca. 6	2,a'	Cu	0.051	17	21	46	49
31 5								-9
21 11	3.3	1,a'	Cu	0.031	17	21	48	-47
30 12	9.0	3,a'	Cu	0.017	22	24	57	53
	2.0	0,a	Mo	0.45	17			
10 19	6.6	1,a'	Cu	0.078	15	19	46	39
	4.4	2,a'	Cu	0.076	17			
31 7								17
20 17	3.4	2,a'	Cu	0.059	11	13	32	-32
22 9								-17
11 18	11	0,a'	Cu	0.068	14	18	45	-41
	16	3,a'	Cu	0.066	15			
31 8	1.1	1,a	Mo	0.50	17	21	51	55
40 1								-0.5
10 20	7.5	1,a'	Cu	0.083	14	17	44	42
	4.0	2,a'	Cu	0.082	14			
40 2	1.5	0,a	Mo	0.54	19	23	60	-53
21 16	6.5	1,a'	Cu	0.055	15	18	49	46

TABLE II. (Continued)

hk-l	I _{obs.}	Layer and Rotation Axis	Radi- ation	A	$\frac{1}{3}\psi$	$\frac{1}{3}\bar{\psi}$ K	$\frac{1}{3}F_0$	$\frac{1}{3}F_2$ u=0.256
40 4	1.4	0,a	Mo	0.53	18	22	58	55
00 21	5.1	0,a'	Cu	0.091	11	13	36	-37
31 10	0.8	1,a	Mo	0.48	14	17	46	-49
40 5								-8
22 12	3.1	0,a'	Cu	0.028	11	13	37	50
30 15	7.9	3,a'	Cu	0.048	10	12	34	30
31 11								23
20 19	4.5	2,a'	Cu	0.071	10	12	34	37
40 7								16
21 17	2.0	1,a'	Cu	0.065	9	11	32	-30
40 8	1.0	0,a	Mo	0.50	18	22	65	52
32 1								-0.3
20 20	4.3	2,a'	Cu	0.078	8.2	10	31	40
32 2	cal.6	1,a'	Cu	0.016	15	18	57	-50
10 22	ca.5.4	1,a'	Cu	0.092	9	9.6	30	-33
	1.7	2,a'	Cu	0.091	7			
31 13	1.1	2,a'	Cu	0.042	5.7	6.9	22	-23
32 4	ca.0.7	2,a	Mo	0.50	15	18	58	53
11 21	11	0,a'	Cu	0.076	10	11	35	-35
	16	3,a'	Cu	0.079	8			
40 10	0.7	0,a	Mo	0.48	15	16	50	-46
	1.0	0,a	Cu		11			
32 5								-8
31 14	6.5	2,a'	Cu	0.054	10	12	41	-42
22 15	3.9	0,a'	Cu	0.064	6	7.2	24	29
40 11								22
21 19	5.6	1,a'	Cu	0.080	8.4	10	35	35
32 7								15
10 23	8.5	1,a'	Cu	0.101	8.8	10	35	40
	5.1	2,a'	Cu	0.101	8.0			
41 0	0.7	1,a	Mo	0.54	15	18	63	52
30 18	11	0,a	Cu		7.3	8.8	31	-38
41 3								7
32 8	ca2.5	1,a'	Cu	0.0143	12	14	52	49
40 13								-22
00 24	6.5	0,a'	Cu	0.104	6.6	8.0	29	32
21 20	8.2	1,a'	Cu	0.089	8.3	10	37	38
20 22	8.0	0,a	Cu		7	8.4	32	-32
41 6	0.5	1,a	Mo	0.500	9	11	41	-46

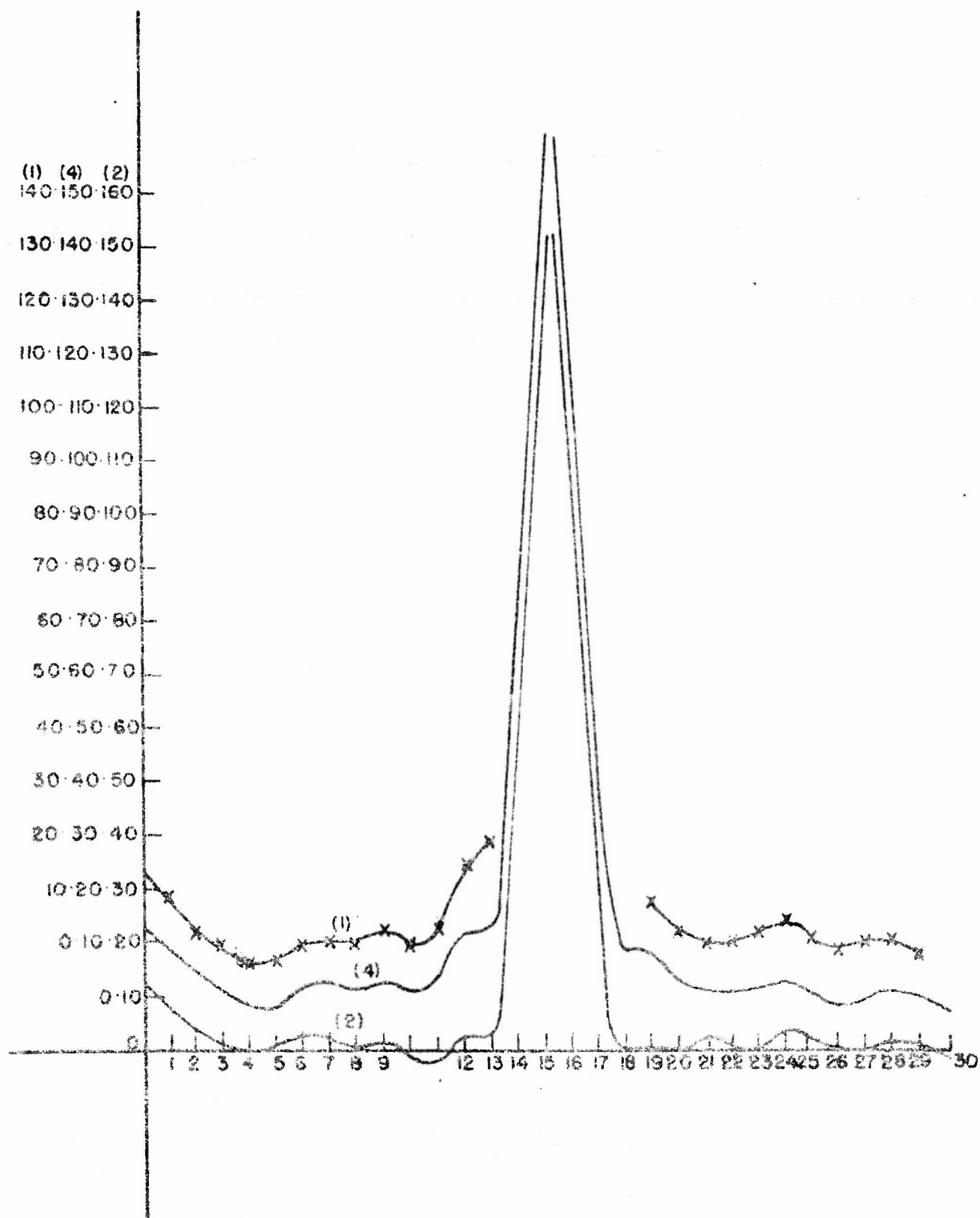


FIG. 5. Electron-Density Line Sections Along the c-Axis from Observed and Calculated Structure Factors.

cesium ion at $z = u \cdot 15.36/60$, the shapes of the cesium peaks on the three line sections are practically the same, although the scale factor, $1/K$, for the observed structure amplitudes, F_o , appears to be slightly too high. However, in the outer shell beyond $r = 0.7\text{\AA}$, the observed electron density, $\rho_o(00z)$, based on either (1), or (4), appears to be considerably higher than $\rho_c(00z)$ based on either (2), or (3). This arises from the fact that the observed values of F_{hk0}^o , F_{hk2}^o and F_{hk4}^o are systematically higher than the calculated values, while the observed values of F_{006}^o , F_{0012}^o , F_{0018}^o , F_{108}^o , F_{1010}^o are considerably lower than the calculated values, because of a higher degree of perfection of the layer crystal along the c-axis and therefore higher extinctions for the $00\frac{1}{2}$ reflections. This point will be discussed later.

It is to be noted that in the outer shell of the cesium ion beyond $r = 0.7\text{\AA}$ the observed electron-density, $\rho_o(00z)$, based on either (1) or (4), appears to be considerably higher on that side of the cesium ion toward the neighboring Cs layer at $z = (\frac{1}{2} - u) = 4.62/60$ than on that side of the cesium ion toward the neighboring O^2 layer at $z = \frac{1}{2} = 20/60$. For $\rho_o(00z)$ based on (1), this difference appears to be most conspicuous in the region between $r = 0.8\text{\AA}$ and $r = 1.1\text{\AA}$; whereas for $\rho_o(00z)$ based on (4), this difference in electron density on the two sides of the cesium ion occurs in the region between $r = 1.4\text{\AA}$ and $r = 2.0\text{\AA}$, in accord with the abnormally large distance between cesium ions in adjacent layers. Since it may not be justifiable to neglect the weak, unobserved reflections and since the agreement between F_o and F_c for most of the weak reflections appears to be good, the observed electron-density line section based on (4) probably gives a better representation of the true relative electron distribution on the two sides of the cesium ion. Based on (2) and (4), the radial distribution difference function, $4\pi r^2(\rho_o - \rho_c)$, appears to be practically symmetrical up to a radius of about 1.4\AA . Between 1.4\AA and 1.7\AA , there are about 8 electrons more in the hemispherical shell towards the neighboring Cs layer (i.e., in the region between $z = 11/60$ and $z = 10/60$) than in the hemispherical shell towards the neighboring oxide layer (i.e., in the regions between $z = 19.7/60$ and $z = 20.7/60$,

assuming hemispherical symmetry of the electron density distribution on both sides of the cesium ion. This difference in electron density on the two sides of the cesium ion gives at least a qualitative indication of the polarization of the cesium ion in the layer lattice; it is of greater significance than the absolute values of $\rho_o(00z)$ in the region between $r = 0.7\text{\AA}$ and $r = 1.4\text{\AA}$, for the apparent high electron density in this region along the c-axis may be largely due to the failure to correct for extinctions in some of the observed structure factors. The eight electron difference has, of course, no quantitative significance although the indication of some degree of polarization seems plausible.

From the observed parameter, $u = 0.256$, and the cell size, $a = 4.256 \pm 0.004\text{\AA}$ and $c = 18.99 \pm 0.02\text{\AA}$, the following interionic distances were obtained: $\text{Cs-O} = 2.86 \pm 0.01\text{\AA}$, $\text{Cs-Cs} = 4.19 \pm 0.02\text{\AA}$.

DISCUSSION

A. Temperature Factor and Lattice Disorder

The fact that the cesium ion appears to be elongated along the c-axis on the observed electron-density line sections would seem to indicate a considerably higher temperature factor along the c-axis than along the a-axis. However, the agreement between F_o and F_c appears to be generally good in the higher $(\sin \theta)/\lambda$ region, where the structure amplitudes are more sensitive to thermal vibrations or other forms of lattice disorder. Hence the effective temperature factor can not be very far from isotropic. In a layer crystal like this, the natural thermal vibration along the c-axis is expected to be higher than along the a-axes, but the effective temperature factor along the a-axes also includes the effect due to the slight layer-shearing disorder. Finally, there may also be a high degree of Schottky disorder in this type of crystal as indicated by the high apparent temperature factor ($B_T = 3.24 \times 10^{-16} \text{cm}^2$).

The powder data show an even higher temperature factor, indicating that disorders due to mechanical

disturbance were not completely removed by annealing. As pointed out previously, the intensities of different types of powder lines of such a layer crystal depend very much on the mechanical treatment of the powder sample. Note that Helms and Klemm⁵ and Brauer¹ reported the powder line intensities for the 10.2, 00.6, and 10.4 reflection as about equal, whereas with a well-annealed powder sample the 10.2 and 10.4 powder lines observed in this laboratory were about four times as strong as the 00.6 powder lines.

B. Extinction Arising from Partial Perfection of the Layer Crystal Along the C-Axis

As pointed out previously, the observed values of $F_{hk.0}^2$, $F_{hk.2}^2$, and $F_{hk.4}^2$ appeared to be systematically higher than the calculated values while the observed values of $F_{00.l}^2$ appeared to be lower. Most of the serious deviations between F_o and F_c occur in the strong reflections in the lower $(\sin \theta) / \lambda$ region. This shows that there were considerable extinctions for the reflections from those lattice planes parallel, or nearly parallel, to the basal plane, as suggested by the fact that the layer crystal of Cs_2O tends to develop perfect basal cleavage and exhibits slight layer-shearing disorder. The crystal might be highly imperfect along the a-axes, but nearly perfect along the c-axis, so that there could be a systematic weakening, because of extinctions, of the strong 00. l reflections and $h0.l$ reflections with small h - and large l -indices. Even small crystallites in the powder sample showed considerable extinctions of these last two types of reflections. The 00.6, 00.12, 10.10 powder lines of a freshly pulverized powder sample of cesium monoxide appeared to be considerably stronger than the corresponding powder lines of an annealed sample (see Fig. 1b), because of further slight cleavage along the basal planes of the crystallites with the resultant decrease in primary extinctions of the 00. l reflections.

C. Polarization of the Cesium Ion in the Layer Lattice

The abnormally large $Cs^+ - Cs^+$ distance

(14.9A vs. $2r_{Cs}^+ = 3.36A$), the slight shortening of the $Cs^+ - O^{2-}$ distance (2.86A vs. $r_{Cs}^+ + r_{O^{2-}} = 1.68A + 1.40A = 3.08A$), and the appreciably higher electron density in the region between $r = 1.4A$ and $r = 1.7A$ on the side of the cesium ion towards the neighboring Cs^+ layer, indicate that the cesium ion must be highly polarized in the cesium monoxide layer crystal by neighboring O^{2-} layer on the one side and the neighboring Cs^+ layer on the other side. Electrostatic repulsion between the two neighboring Cs^+ layers is also expected to increase the $Cs^+ - Cs^+$ distance. A theoretical justification of the abnormally large $Cs^+ - Cs^+$ distance based on the combined effect of polarization and electrostatic repulsion can be made by expressing the lattice energy of cesium monoxide as a function of the parameter, u , knowing the cell size and the polarizability of the cesium ions; this lattice energy could then be compared with that calculated from known thermochemical¹⁰ and spectroscopic data by means of the Born-Haber cycle.*

* The Madelung constant for the Cs_2O crystal has been calculated for each of several values of the parameter u in the vicinity of 0.256. The electrostatic (Coulomb) contribution to the lattice energy is thereby obtained. For the observed value of $u = .256$ the electrostatic contribution to the dissociation energy (into ions) is found to be +531.7 Kcal. while that calculated from the observed heat of formation of Cs_2O using the Born-Haber cycle is +528.5±7 Kcal. This close agreement suggests that the (non-Coulombic) repulsive energy is very nearly compensated by the polarization energy (due to polarization of cesium ions) and the Van der Waals attraction. The non-Coulombic repulsion and the polarization energies have also been calculated. As expected, the polarization energy is opposite in sign to the repulsion and cancels about two thirds of it. The Van der Waals energy has not been computed but it seems reasonable that it will nearly cancel the remainder of the non-Coulombic repulsion. Some further calculations seem required in order to produce a finished piece of work. Since most of the above calculations were performed after termination of the contract and since the calculations are still in progress the details are not being reported. It is now quite clear, however, that Cs_2O is a perfectly normal ionic crystal. The unusual structure may well be due to the high polarizability of cesium ion although this is not yet unambiguously proven by calculation.

It is to be noted that, in the case of the cadmium chloride type layer crystals, the polarizing field acting on the halide ions is reversed in direction and tends to draw electrons away from the region between the halide-halide layers, while the electrostatic repulsion still tends to keep the two neighboring halide layers apart. Thus the two effects now more or less compensate, rather than reinforce, each other. Hence the observed halide-halide interionic distances in the CdCl_2 -type of layer crystals appear to be normal in the case of the chlorides and the bromides (Table III). However, in the case of the nickel iodide layer crystal, the observed $\text{I}^- - \text{I}^-$ distance 3.97\AA is about 0.35\AA lower than twice the known ionic radius (2.16\AA) of the iodide ion. This indicates that for the large iodide ion, the polarization effect actually predominates as should be expected.

D. Extra Powder Lines of Impure Cesium Monoxide Sample

A sample of cesium monoxide known to contain 2.8% excess oxygen gave the following extra powder lines: $d/n = 3.80(5)$, $3.60(2)$, $3.06(2)$, $2.60(3)$, $2.44(1)$; figures inside the brackets indicate the observed intensities relative to that of the strongest Cs_2O powder line (10.2-line) as 100. Other powder samples of Cs_2O known to be partially oxidized because of inadequate purification of the argon also showed these extra lines together with three more foreign lines at $d/n = 1.92(1)$, $1.88(1)$, and $1.62(1)$. These extra lines cannot be indexed by the known Cs_2O pattern, or Cs_2O_3 pattern, or a combination of both. Furthermore, the oxygen-rich impurities did not appear to be paramagnetic since the impure Cs_2O sample still showed practically the same diamagnetic susceptibility as that of an almost stoichiometric sample. The existence of a diamagnetic higher oxide, probably Cs_2O_2 , is indicated^{1,9}. Difficulty of preparing such an intermediate higher oxide of cesium in a sufficiently pure state arises from the fact that, in the solid-gas reaction between cesium monoxide and oxygen, once a thin surface coating of the intermediate higher oxide is formed it is oxidized further to Cs_2O_3 and CsO_2 while the interior layer of unreacted Cs_2O remains shielded from the action of oxygen.

TABLE III. INTERATOMIC DISTANCES OF Ca_{20}
AND CdCl_2 -TYPE LAYER CRYSTALS

Layer Crystals	Cell Constants		Parameter u	Interatomic Distances		Interatomic Distance calculated $\frac{d}{d_0} = 2r$
	Rhombohedral a_0 (Å)	Hexagonal a (Å) c (Å)		observed d_1 (Å)	d_2 (Å)	
CdCl_2	6.23	36°21'	0.25	2.66	3.66	
CoCl_2	6.16	33°26'	0.25	2.51	3.56	
FeCl_2	6.20	33°33'	$\frac{1}{2}$ (?)	2.53	3.58	
NiCl_2	6.22	33°36'	$\frac{1}{2}$ (?)	2.54	3.59	3.60±0.04Å
MnCl_2	6.20	34°35'	$\frac{1}{2}$ (?)	2.58	3.61	
NiCl_2	6.13	33°36'	$\frac{1}{2}$ (?)	2.51	3.55	
ZnCl_2	6.31	34°48'	$\frac{1}{2}$ (?)	2.63	3.67	
NiBr_2	6.465	33°20'	0.255	2.58	3.88	3.90Å
CdBr_2	6.63	34°22'	$\frac{1}{2}$ (?)	2.77	3.86	
NiI_2	6.92	32°40'	0.250	2.78	3.97	4.32Å
Ca_{20}	6.79	36°32'	0.256	2.86	4.19 (d_1)	3.38Å(d_1)
	6.74	36°56'	$\frac{1}{2}$ (?)	2.91	3.99 (d_1)	H. & K.

Note: The observed interatomic distances of the CdCl_2 -type layer crystals were calculated from the corresponding cell constants and parameters given in Wyckoff's "Crystal Structures" vol. I, Table IV, 7 (1948). For the Ca_{20} layer crystal, the observed cell constants, parameter, and interatomic distances listed above are based upon the present determination with Helms and Klemp's observed values listed below for comparison. The calculated interatomic distances for X-X and Ca-Og are based upon Pauling's crystal radii.

SUMMARY

1. The x-ray powder pattern of cesium monoxide has been re-examined. The presence of many powder lines (weak) with odd hexagonal l -indices shows that the Cs^+ ions cannot be in a body-centered rhombohedral setting and therefore the parameter $u = 1/4$, given by Helms and Klemm, is incorrect.

2. Single crystals of cesium monoxide have been prepared for the first time. Single-crystal photographs have confirmed the anti- CdCl_2 -type layer structure, D_{3d}^2 . Rotation photographs have been found to show the existence of layer-shearing disorder in the crystal, similar to that exhibited by brucite, $\text{Mg}(\text{OH})_2$, a layer crystal, recently discussed by Brindley and Ogilvie². Layer-shearing disorder in the Cs_2O crystals has also been observed on the powder photograph taken with a freshly pulverized sample.

3. Treatment of the single-crystal data for absorption corrections by direct integration has been described in some detail. High extinctions for the strong $00l$ reflections and $h0l$ reflections with small h - and large l -indices have been observed, arising from more or less perfect basal cleavage and slight layer-shearing disorder.

4. The cell constants and interionic distances have been found to be: $a = 4.256 \pm 0.004 \text{ \AA}$, $c = 18.99 \pm 0.02 \text{ \AA}$, $u = 0.256$; $\text{Cs}^+ - \text{O}^{2-} = 2.86 \pm 0.01 \text{ \AA}$, $\text{Cs}^+ - \text{Cs}^+ = 4.19 \pm 0.02 \text{ \AA}$.

5. A differential comparison of the observed and the calculated electron-density line section along the c -axis indicates that the cesium ions are polarized in the layer lattice of cesium monoxide crystals.

6. The abnormally high $\text{Cs}^+ - \text{Cs}^+$ distance has been ascribed to the combined effects of the polarization of the cesium ions and the electrostatic repulsion between adjacent Cs^+ layers. Interionic distances in the CdCl_2 -type layer crystals have also been discussed in the light of these two effects.

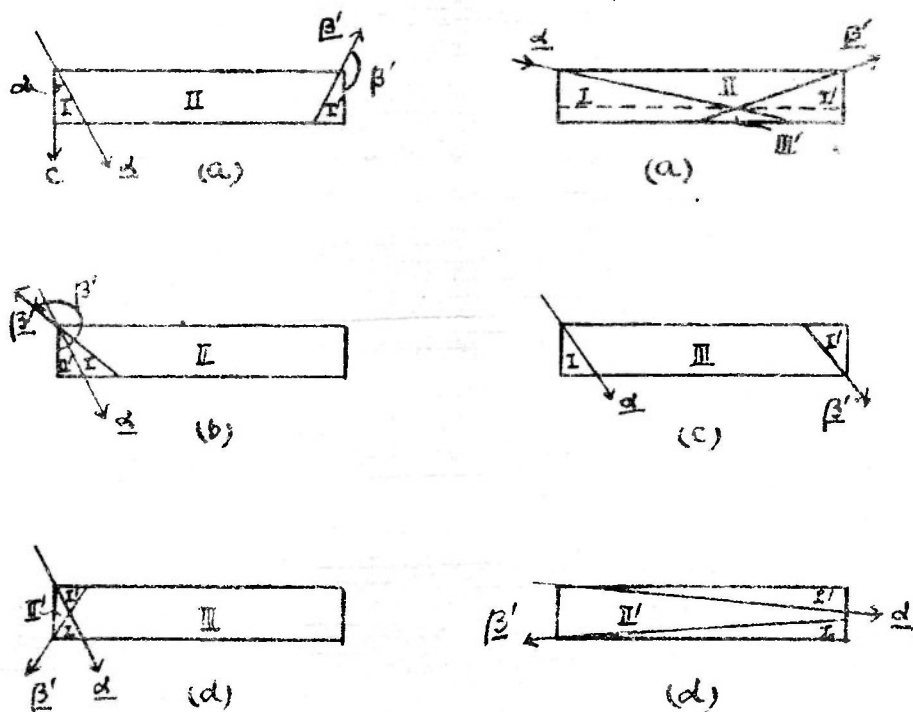
7. Extra powder lines of partially oxidized powder samples of cesium monoxide and the observed diamagnetic susceptibility of the sample suggest the existence of an intermediate higher oxide besides CsO_2 and Cs_2O_3 (?).

APPENDIX

CALCULATION OF THE ABSORPTION FACTOR BY DIRECT INTEGRATION

A. Rotation about the Base Diagonal, (11·0).
The axis of rotation being parallel to the vertical edges of the crystalline plate, the case of one of constant cross section except for the upper and lower edges (and the small truncated corner which can be neglected).

If the c-axis is taken as the polar axis, then the direction of the incident beam, α , can be confined to the first quadrant without loss of generality, and the projected direction of the diffracted beam, β' , may lie in one of the four quadrants. The cross section of the crystal plate can be divided into appropriate regions for integration as shown in the following diagram:



These regions can be designated as regions of corner reflections, I and I', surface reflections, II and II', and internal reflections, III and III', the contribution for the last one being negligible. The absorption factor, A, can be obtained by integrating the following expression:

$$A = \frac{h}{V} \sum_i \int_{S_i} e^{-\mu(x_1 + x_2)} dS_i$$

$$= \frac{h}{V} \sum_i \int_{S_i} e^{-\mu(x_1 + x_2' \sec \chi)} dS_i$$

where μ , v , s , and h are, respectively, the absorption coefficient, the volume, the cross section area, and the height of the crystal; x_1 and x_2 are the optical paths of the incident and diffracted beams; x_2' is the projection of the diffracted beam, x_2 , upon s ; χ is the layer inclination angle; and the summation is to be carried out over all the separate regions, S_i . After simplification, the following expressions are obtained:

(a) α and β in the first and second quadrants.

$$A = \frac{h}{V} \left\{ \frac{\sin(\alpha + \beta') \cos \chi}{\mu^2} \left(1 - \frac{\cos \alpha \cos \beta}{(\cos \alpha + \cos \beta)^2} \right) \right.$$

$$\left. - \frac{\sin \alpha + \sin \beta' \cos \chi}{\mu^2} \cdot \frac{\cos \alpha \cos \beta}{(\cos \alpha + \cos \beta)} + \frac{l \cos \alpha \cos \beta}{\mu \cos \alpha + \cos \beta} \right\}.$$

Special case: $\alpha = \beta = \beta'$, $\chi = 0$;

$$A = \frac{h}{V} \left(\frac{l}{2\mu} \cos \alpha + \frac{\sin 2\alpha}{4\mu^2} \right).$$

(b) α and β in the first and third quadrants.

$$A = \frac{h}{V} \left\{ \frac{l \cos \alpha \cos \beta}{\mu \cos \alpha + \cos \beta} + \frac{1}{\mu} \frac{\sin \alpha \sin \beta' \cos \chi}{\sin \alpha + \sin \beta' \cos \chi} \right.$$

$$+ \frac{\sin \beta' \cos \chi}{\mu^2} \cdot \left(\frac{1}{\cos \alpha} + \frac{1}{\sin \beta' \cos \chi} \right)$$

$$\left. - \frac{\sin \beta' \cos \chi}{\mu^2} \cdot \left(\frac{1}{\cos \alpha} + \frac{1}{\cos \beta} \right) \right\}, \quad \beta' > \alpha;$$

or

$$A = \frac{h}{V} \left\{ \frac{l}{M} \frac{\cos \alpha \cos \beta}{\cos \alpha + \cos \beta} + \frac{t}{M} \frac{\sin \alpha \sin \beta' \cos \chi}{\sin \alpha + \sin \beta' \cos \chi} \right. \\ \left. + \frac{\sin \alpha}{M^2} \div \left(\frac{1}{\cos \beta} + \frac{\tan \beta'}{\sin \alpha} \right) \right. \\ \left. - \frac{\sin \alpha}{M^2} \div \left(\frac{1}{\cos \alpha} + \frac{1}{\cos \beta} \right) \right\}, \\ \text{for } \beta' < \alpha.$$

(c) α and β' in the first quadrant.

$$A = \frac{h}{V} \left\{ \frac{l}{M} \left[\exp\left(-\frac{Mt}{\cos \alpha}\right) - \exp\left(-\frac{Mt}{\cos \beta}\right) \right] \div \left(\frac{1}{\cos \beta} - \frac{1}{\cos \alpha} \right) \right. \\ \left. + \frac{\sin(\alpha + \beta') \cos \chi}{M^2} \right\} + \frac{1}{V} \times \frac{2l \cos \alpha \cos \beta}{M^2 \cot \gamma},$$

the last term being the correction for internal reflection through the upper and lower edges with $T10\gamma$ -plane as the inclined surface, and γ being the angle between the c-axis and the $T10\gamma$ -plane.

(d) α and β' in the first and fourth quadrants.

$$A = \frac{h}{V} \left\{ \frac{l}{M} \left[\exp\left(-\frac{Mt}{\cos \alpha}\right) - \exp\left(-\frac{Mt}{\cos \beta}\right) \right] \div \left(\frac{1}{\cos \beta} - \frac{1}{\cos \alpha} \right) \right. \\ \left. + \frac{t}{M} \div \left(\frac{1}{\sin \alpha} + \frac{1}{\sin \beta' \cos \chi} \right) \right. \\ \left. + \frac{\sin \alpha}{M^2} \div \left(\frac{1}{\cos \beta} + \frac{\tan \beta'}{\sin \alpha} \right) \right. \\ \left. + \frac{\sin \beta' \cos \chi}{M^2} \div \left(\frac{1}{\cos \alpha} + \frac{\tan \alpha}{\sin \beta' \cos \chi} \right) \right\} \\ + \frac{1}{V} \times \frac{2l \cos \alpha \cos \beta}{M^2 \cot \gamma}.$$

In the above expressions, α , β , and β' are taken as the acute angles which α , β , and β' , respectively, make with the c-axis. The crystal is treated as a rectangular plate except for the two $\bar{1}104$ -edges, the small truncated corner being neglected.

B. In the case of rotation about the hexagonal a-axis (10.0), the crystal plate can be divided by horizontal planes passing through the corners into a central parallelogized section with constant horizontal cross section, and a top and a bottom section where the width, l , varies with the height because of the triangular faces. Integration of the absorption factors for these sections is still quite straightforward, except that, for $\text{MoK}\alpha$ radiation, the exponential terms can no longer be neglected because of the considerably smaller absorption coefficient ($\mu=190\text{cm}^{-1}$ for $\text{MoK}\alpha$, and $\mu=1520\text{cm}^{-1}$ for $\text{CuK}\alpha$, based upon the mass absorption coefficients of Cs and O given in Int. Tabellen, II, 577 - 78 (1935), and the known density of the crystal, 4.70g/cc.). However, for α and β' less than 60° , good approximations for the absorption factors can be obtained by merely integrating through the thickness of the crystal plate and neglecting all the corner and edge corrections:

$$A = \frac{1}{V} \int_V e^{-\mu(x_1+x_2)} dV \approx \frac{1}{t} \int_0^t e^{-\mu(x_1+x_2)} dt$$

The $\text{CuK}\alpha$ photograph taken with the hexagonal a-axis as the rotation axis was used only in checking some of the unresolved reflections on the other two photographs. The relative magnitudes of the absorption factors were estimated from the values calculated for the corresponding reflections on the base-diagonal rotation photograph using the same radiation.

For each reflection, the angles α and β' , which the incident beam and the projection of the diffracted beam, respectively, make with the c-axis, were determined graphically with the use of a reciprocal lattice map and a circle of reflection for the appropriate layer. The angle, β , between the diffracted beam and the c-axis can be obtained from the following relation: $\cos\beta = \cos\beta' \cos\chi$, where χ is the layer inclination angle. It is to be noted that, for those reflections above the zero layer with β -factor greater than 1, there are two pairs of α and β , and therefore two values of the absorption factor, A , for each reflection. In

such cases, mean values of A were taken.

For fixed hk , the absorption factor, $A_{hk \cdot \varrho}$, can be plotted as a function of ϱ . This is illustrated in Fig. 4 for the case of rotation about the base diagonal, $(11 \cdot 0)$, and with $\text{CuK}\alpha$ radiation. A change in the type of reflection is indicated by an abrupt change in the slope of the absorption curve.

REFERENCES

1. Brauer, V.G., Zeit. anorg. Chem. 255, 101 (1947).
2. Brindley, G.W. and Ogilvie, G.J., Acta Cryst. 5, 412 (1952).
3. Centnerswer, M. and Blumenthal, M., Bl. Acad. Polon. A 1933, 305 (1933); C.A. 1934, 2729 (1934).
4. Helms, A. and Klemm, W., Zeit. anorg. Chem. 241, 97 (1939).
5. Helms, A. and Klemm, W., ibid., 242, 33 (1939).
6. Helms, A. and Klemm, W., ibid., 242, 201 (1939).
7. Hendershot, O.P., Rev. Sci. Instr. 8, 324 (1937).
8. Howells, R.G., Acta Cryst. 3, 366 (1950).
9. Rengade, E., Ann. Chem. Phys. 11, 348 (1907); Bull. Soc. Chem. and Phys. 39, 667 (1907).
10. Rengade, E., Ann. Chem. Phys. 14, 540 (1908).
11. Terry, H. and Diamond, H., J. Chem. Soc. 1928, 2820 (1928).
12. Wyckoff, R.G.W., "Crystal Structures", vol. I, chapter IV, 11, Interscience Publishers, N.Y. (1948).

NOTE: In submitting this report it is understood that all provisions of the contract between The Foundation and the Cooperator and pertaining to publicity of subject matter will be rigidly observed.

Investigator K.M. Huey Tsai Date

Supervisor F.N. Lewis Date Sept. 15, 1953

For The Ohio State University Research Foundation

Executive Director Oram C. Woolpert Date 16 Sept. 1953
W.K.H.